Journal of Materials Chemistry A

PAPER

View Article Online
View Journal | View Issue

Published on 30 April 2015. Downloaded by University of Connecticut on 09/07/2015 16:10:22.

Cite this: J. Mater. Chem. A, 2015, 3, 14845

Rational design and synthesis of polythioureas as capacitor dielectrics†

Rui Ma,[a] Vinit Sharma,[b] Aaron F. Baldwin,[a] Mattewos Tefferi,[c] Ido Offenbach,[d] Mukerrem Cakmak,[d] Robert Weiss,[d] Yang Cao,[c] Rampi Ramprasad[b] and Gregory A. Sotzing*[ae]

Received 15th February 2015
Accepted 17th April 2015

DOI: 10.1039/c5ta01252j

www.rsc.org/MaterialsA

Rational strategies combining computational and experimental procedures accelerate the process of designing and predicting properties of new materials for a specific application. Here, a systematic study is presented on polythioureas for high energy density capacitor applications combining a newly developed modelling strategy with synthesis and processing. Synthesis was guided by implementation of a high throughput hierarchical modelling with combinatorial exploration and successive screening, followed by an evolutionary structure search based on density functional theory (DFT). Crystalline structures of polymer films were found to be in agreement with DFT predicted results. Dielectric constants of ~4.5 and energy densities of ~10 J cm^{-3} were achieved in accordance with Weibull characteristic breakdown fields of ~700 MV m^{-1}. The variation of polymer backbone using aromatic, aliphatic and oligoether segments allowed for tuning dielectric properties through introduction of additional permanent dipoles, conjugation, and better control of morphology.

Introduction

Electrical energy storage devices are indispensable components in modern electronics.[1–4] It is always important but challenging, to explore new materials to fulfil the demand of their continuous miniaturization and improved functionality.[5–7] Among these devices, which include batteries, supercapacitors, fuel cells, *etc.*, parallel plate capacitors offer high power density but low energy density. Therefore, it is essential to improve their performance by designing new dielectric materials with high capacitive energy density.[8–11] To maximize the energy density, a desirable dielectric should exhibit high dielectric constant (K), high breakdown strength, and low loss during charge–discharge cycles. The current state-of-the-art polymer dielectric film, biaxially oriented polypropylene (BOPP)[12–16] has a breakdown strength of 730 MV m^{-1} and low dielectric loss (tan δ ~ 0.0002 at 1 kHz, r.t.), but suffers from a low dielectric constant of 2.2 and a reduced breakdown strength and cycle life at temperatures in excess of 85 °C.

Many approaches have been taken to enhance energy density by increasing K and breakdown field through the use of materials such as polymer nanocomposites, modified ferroelectric crystalline polymers, and amorphous polar polymers with low loss. Nanoparticle fillers[17–20] are effective at increasing K but are limited to high percolation volume% necessary for achieving increased energy density, as well as the issue of agglomeration.[21,22] PVDF and their copolymers have been a focus for recent research,[23–25] however the coercivity inherent to ferroelectrics results in high loss. Recently, the approach on developing amorphous polar polymers, such as polyimides,[26–28] polyurethanes, polyureas[29] and polythioureas[30] took over the thought of utilizing dipolar (orientational) polarization for high K,[31] as well as minimizing nonlinear behaviour originating from highly oriented polar polymer chains. Our team explored chemical space to incorporate tin covalently into polymer chain and achieved increased dielectric constant and band gap.[32]

These processes of design and selection are dominated by trial and error strategies guided by intuition, which could be significantly more efficient by using the tools of advanced computational screening. We recently proposed a hierarchical modelling strategy[29,33] to accelerate the identification of polymer dielectrics with successive downselection steps: combinatorial chemical space exploration using four independent building blocks; identification of promising repeat unit based on band gap and dielectric constant estimates; 3D structure predictions of polymers composed of the downselected repeat

[a]Polymer Program, University of Connecticut, 97 North Eagleville Rd, Storrs, CT 06269, USA
[b]Department of Materials Science and Engineering, University of Connecticut, 97 North Eagleville Rd, Storrs, CT 06269, USA
[c]Department of Electrical and Computer Engineering, University of Connecticut, 97 North Eagleville Rd, Storrs, CT 06269, USA
[d]Department of Polymer Engineering, University of Akron, 250 South Forge St, Akron, Ohio 44325, USA
[e]Department of Chemistry, University of Connecticut, 97 North Eagleville Rd, Storrs, CT 06269, USA

† Electronic supplementary information (ESI) available. See DOI: 10.1039/c5ta01252j

Published on 30 April 2015. Downloaded by University of Connecticut on 09/07/2015 16:10:22.

units; property predictions of the 3D systems. Combined with experimental results, we determined polythiourea as one of the promising systems with a repeat unit of –NH–CS–NH–C_6H_4–. The polymer has a simple structure beneficial for calculation process, but it showed limited solubility and processability. Therefore, further modification and optimization needs to be conducted on the experimental side.

Here, a systematic synthesis and processing study on polythiourea was conducted in combination with our hierarchical modelling strategy to provide a clear structure – dielectric property relationship. To further improve the dielectric property and processability, different chain segment including aromatic, aliphatic and oligoether with various additional dipoles were incorporated into the basic polythiourea backbone. Scalable synthetic procedures were one of the materials selection criteria making these systems the potential candidates for industrial scale manufacturing of thin films and capacitor assembling.

Results and discussion

1. Systematic synthesis and thermal properties

Molecular structures were inspired by a simple polythiourea structure identified by calculation results.[29] The polymer with a repeat unit of –NH–CS–NH–C_6H_4– (also listed here as PDTC-PhDA) showed promising dielectric properties, but had limited solubility and processability in that it only dissolved in hot DMSO, and only low molecular weights were achieved due to early precipitation during a condensation polymerization.

With the exception of one synthesis, polymerizations shown in Scheme 1 were carried out by the reaction of a diamine with a diisothiocyanate. In order to reproduce the polythiourea reported by Wu *et al.*,[30] polymerization was carried out between a diamine and thiophosgene, which can be scaled up with a reasonable cost. Polymers precipitated out of the reaction solution in the form of white fibres, which was a first indication that these polymers had achieved a high degree of polymerization. The polythioureas were characterized by proton nuclear magnetic resonance spectroscopy (^{1}H-NMR), infrared spectroscopy (IR), and powder X-ray diffraction for structure determination and by thermogravimetric analysis (TGA), and differential scanning calorimetry (DSC) for thermal properties. The number average molecular weight reported in Table 1 was calculated using end group analysis from ^{1}H-NMR (see ESI† for details of synthesis and characterizations). All newly synthesized polythioureas showed high molecular weight (Table 1) and improved solubility compared to PDTC-PhDA.[29] PDTC-MDA, PDTC-HDA and PDTC-HK511 are soluble in *N*,*N*-dimethylformamide (DMF), *N*,*N*-dimethylacetamide (DMAc), dimethyl sulfoxide (DMSO) and *N*-methylpyrolidinone (NMP). In addition to these solvents, PDTC-HK511 is also soluble in tetrahydrofuran (THF). PDTC-ODA and thiophosgene-MDA, on the other hand, show limited solubility in DMF, DMAc and NMP, but a good solubility in DMSO at room temperature. Thermal properties play an important role in polymer thin film processing and dielectric properties at elevated temperature. The occurrence of a phase transition, such as a glass transition, within the operating temperature range of a capacitor can be detrimental since polymer chain segmental motion increases dielectric loss, and reduces energy storage efficiency. PDTC-HDA and PDTC-HK511 show glass transition temperatures of 139 °C and 92 °C, respectively, due to flexible chain segments. All other polythioureas did not exhibit any observable T_g, and, generally have high degradation temperatures.

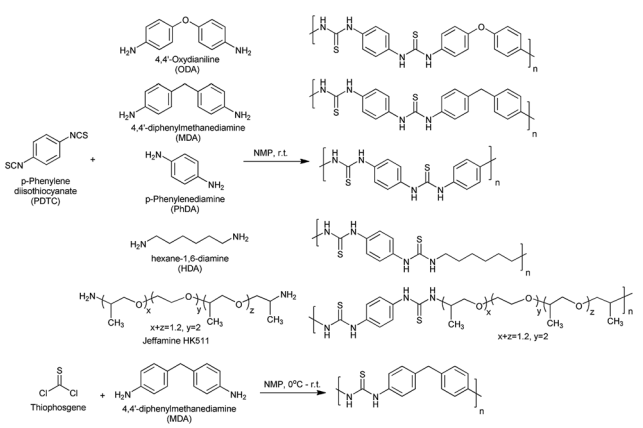

Scheme 1 Polythiourea synthetic route and structures.

2. Structure/morphology exploration and dielectric properties

From rational design, polythiourea was identified to have desirable electrical properties from a first level screen involving a 1-dimensional catenation of repeat units into a polymer chain.[29] The second step of determining a 3-dimensional structure helped to provide more accurate prediction of dielectric properties. The structure search was conducted with an evolutionary algorithm based method[34–36] specially modified to handle repeat units rather than atoms as the building blocks using DFT energetics. The same approach was applied here for the rational design of polythioureas containing different chain segments.

To predict the crystal structure of these polymers we applied a constrained evolutionary search algorithm embodied in USPEX code where each monomeric unit is treated as one motif with fixed connectivity. During the course of evolutionary optimization, fixing the chemical connectivity greatly reduces the search space and allows the initial structure generation with different packing to identify the most stable packing of monomers. The diversity in initial structures is maintained by

Table 1 Molecular weight and thermal properties

Polymer	M_n (g mol^{-1})	T_g (°C)	T_d (°C)
PDTC-ODA	21 500	N/O	246
PDTC-MDA	56 400	N/O	228
PDTC-PhDA	N/A	N/O	276
PDTC-HDA	85 100	139	275
PDTC-HK511	25 900	92	294
Thiophosgene-MDA	44 600	N/O	311

 This journal is © The Royal Society of Chemistry 2015

Published on 30 April 2015. Downloaded by University of Connecticut on 09/07/2015 16:10:22.

allowing a certain degree of variation in the rotation and translation of polymers along the chain direction. Low energy configurations of the polymers were identified and further studied for computing the electronic and dielectric properties. The predicted low energy crystal structures as well as the corresponding infrared (IR) spectra and X-ray diffraction (XRD) patterns, all numerically computed, are shown in Fig. 1, along with the experimentally determined IR spectra and XRD

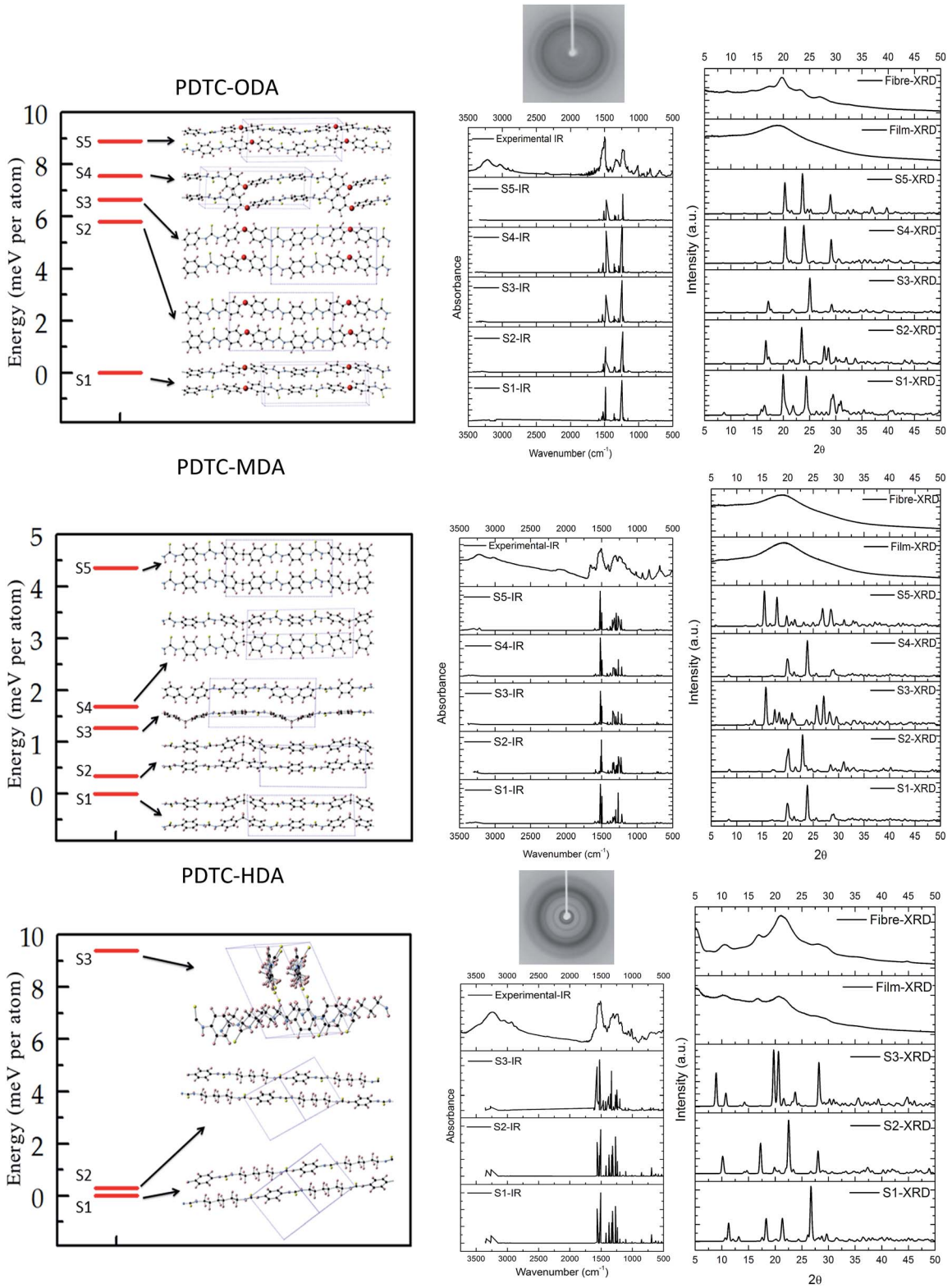

Fig. 1 Calculated and experimental structures of PDTC-ODA (top), PDTC-MDA (middle) PDTC-HDA (bottom).

Published on 30 April 2015. Downloaded by University of Connecticut on 09/07/2015 16:10:22.

patterns. For each predicted crystal structure, the numerically calculated values of the band gap (E_g), total (K_t) and electronic (K_e) part of dielectric constants for PDTC-ODA, PDTC-MDA, and PDTC-HDA are summarized in Table 2, along with experimentally determined band gap (E_g), total (K_t) dielectric constant. The measured electronic (K_e) part of dielectric constant was determined indirectly from the refractive index measured from the ellipsometry.

The correspondence between the measured IR spectrum and that of the predicted structures is uniformly good, except for some details that are not able to be shown in experimental results. The IR peaks are dominated by chemical bonds and hence consistently reproduced for all predicted structures to show similar IR spectrum. In terms of morphology, PDTC-HDA fibre and film are both semicrystalline, whose XRD diffraction pattern is in agreement with predicted structure S2 (Fig. 1, bottom), computationally identified as one of the structures with lowest energy. Dielectric constants are close for all three computationally derived structures. With regards to the discrepancy in the calculated and experimentally derived dielectric constants, the experimental dielectric constant values reflect an average of both amorphous and crystalline phases, whereas the calculated structures represent only the purely crystalline form (Table 2). After solution processing, PDTC-ODA films were found to be amorphous (Fig. 1, top), whereas fibres show an obvious diffraction pattern, similar to that of predicted structure 1. Therefore, the lower dielectric constant for the film *versus* the value derived from computation is expected. PDTC-MDA (Fig. 1, middle) is amorphous in both fibre and film as that there is no significant XRD diffraction pattern. All polymers show high refractive indices due to the presence of both aromaticity and sulphur. Aliphatic polythioureas exhibit a lower refractive index than their aromatic analogues. With refractive indices as high as 1.81 for solution casted colourless films, these polythioureas could be promising for optical devices.[37]

Dielectric properties were evaluated experimentally in terms of dielectric constant, loss, band gap, DC breakdown strength, and charge–discharge behaviour determined from a *D–E* hysteresis loop. Dielectric constant and dissipation factors (tan δ) are listed in Table 3. Dielectric constants are all higher than BOPP, and comparable with the polythiourea reported recently by Wu *et al.*[30] Higher dielectric constants were achieved by addition of permanent dipoles such as diphenyl ether, and oligoether segments which enhance polarization, resulting in higher dielectric constants for PDTC-ODA and PDTC-HK511. Dielectric constant increases with increasing conjugation length, which is attributed to the enhanced π electron mobility.

Table 3 Dielectric properties, experimental

Polymer	K (r.t. 1 kHz)	tan δ (r.t. 1 kHz)	E_g (eV)	Refractive Index
PDTC-ODA	4.52	0.0233	3.22	1.79
PDTC-MDA	4.08	0.0348	3.16	1.81
PDTC-PhDA	4.89	0.0144	3.07	N/A*
PDTC-HDA	3.67	0.0267	3.53	1.71
PDTC-HK511	6.09	0.0115	3.51	1.64
Thiophosgene-MDA	3.84	0.0226	3.30	1.74

Even with the high dielectric constant, and increased conjugation in these systems, tan δ remains at approximately 2% which is also comparable to the loss factor reported recently for other polythioureas.[30]

Dependence of K and tan δ on temperature and frequency were evaluated by time domain dielectric spectroscopy, with PDTC-MDA and PDTC-HDA being representative examples

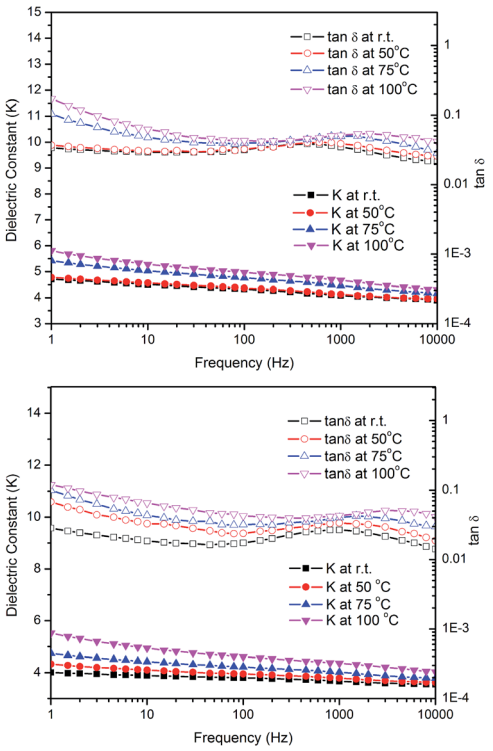

Fig. 2 Dielectric Spectrum of PDTC-MDA (top) and PDTC-HDA (bottom).

Table 2 Dielectric properties: predicted structure and experiment (Exp.)

	PDTC-ODA						PDTC-MDA						PDTC-HDA			
Crystal structure	S1	S2	S3	S4	S5	Exp.	S1	S2	S3	S4	S5	Exp.	S1	S2	S3	Exp.
E_g (eV)	3.31	3.07	3.06	3.44	3.45	3.22	3.25	3.69	3.47	3.25	3.41	3.16	3.68	3.81	3.77	3.70
K_e	3.78	3.94	3.90	3.86	3.84	3.20	3.31	3.71	3.78	3.88	3.79	3.28	3.33	3.35	3.18	2.92
Refractive Index	—					1.79	—					1.81	—			1.69
K_t	5.68	5.05	6.81	4.82	4.74	4.52	4.08	4.35	4.52	4.83	5.15	4.08	3.98	4.00	4.05	3.67

This journal is © The Royal Society of Chemistry 2015

Published on 30 April 2015. Downloaded by University of Connecticut on 09/07/2015 16:10:22.

shown in Fig. 2 (spectra for the other polythioureas are reported in ESI†). The dielectric constant increases as temperature increases due to improved chain mobility, which enhances the dipole alignment along the applied electric field. However, in the high frequency regime, the dielectric constant slowly decreases due to relatively slow segmental motion of dipoles in the polymer chain. In general, dielectric constant remains steady over a wide frequency range suggesting a relatively fast polarization response. tan δ shows a weak peak at *ca.* 1 kHz, however remains relatively low throughout the frequency range tested. As temperature increases tan δ slightly increases and this peak shifts to higher frequencies, which can be explained by increased dipole mobility.

The energy density is proportional to the square of the electric field and therefore is limited by the breakdown field of the polymer dielectric. By operating at a high electric field, the significantly higher energy density can be achieved. The fundamental mechanism of polymer breakdown lies in the electronic breakdown, which is often explained by electron avalanche theory.[38] Band gap is believed to be the basic property related to the intrinsic breakdown where a larger band gap implies a higher threshold for impact ionization. The band gaps of polythiourea, that are highly dependent upon chemical structure, were evaluated by UV absorption (Table 3). The highest band gap was achieved for polythioureas containing aliphatic segments whereas the presence of extensive π conjugation lowers the band gap due to electron delocalization. The higher band gap of PDTC-HDA, and HK511 implies a higher intrinsic breakdown strength than that for PDTC-ODA and PDTC-MDA.

However, the measured engineering DC breakdown is shown to differ, as PDTC-ODA, MDA have a higher breakdown field than PDTC-HDA. First, the relationship of band gap and intrinsic breakdown is not well established for polymer, much worse for engineering breakdown strength which is dominated by "extrinsic" factors not inherent to the material such as imperfections (*e.g.*, chemical impurities at the atomic level, and cavities at the microscopic and macroscopic scales) as well as statistical variations in morphology and microstructure. Second, polymer breakdown phenomenon also depends on other mechanisms besides electronic breakdown including thermal breakdown, partial charge and free volume breakdown.[39] It has been proposed that the presence of random dipoles in amorphous polar polymers provide electron–dipole scattering in addition to electron–phonon scattering to stabilize electron energy and hence, prevent dielectric breakdown.[40] Here

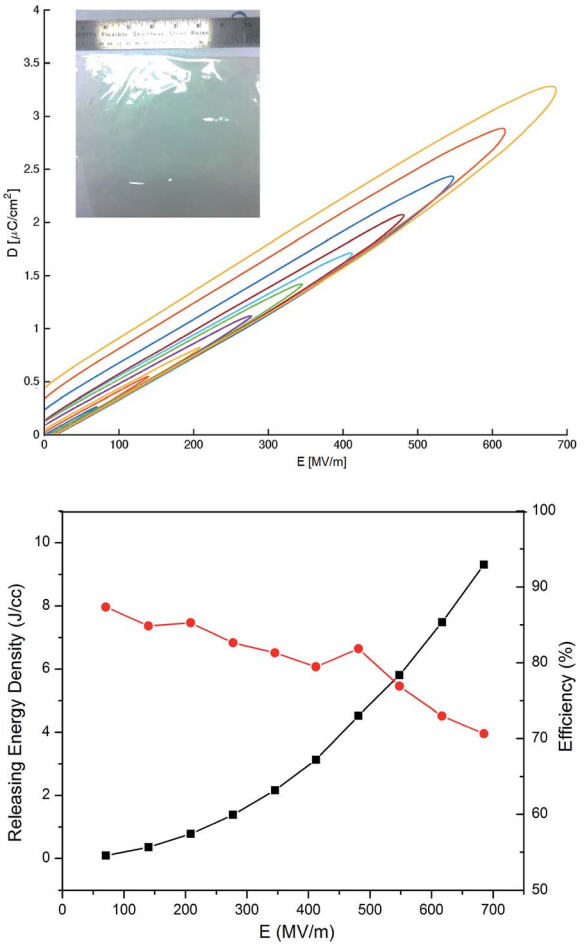

Fig. 3 *D*–*E* hysteresis loop for PDTC-HDA.

for the polythiourea systems, amorphous films of PDTC-ODA and PDTC-MDA show higher dc breakdown voltages than the semicrystalline films of PDTC-HDA confirming that there might be an advantage to polar polymers being in an amorphous state. Another advantage is that the amorphous material is more homogenous than a semicrystalline one, and fluctuations of electrical properties will occur on a much smaller scale. The breakdown field of PDTC-HK511 is lower than all the other polythioureas due to poor film quality. The T_g of PDTC-HK511 is lower than the drying temperature of the film causing unevenness and defects in the free-standing films that were obtained.

Charge–discharge behaviour was estimated using *D*–*E* hysteresis loop. Film samples were prepared in the same way as

Table 4 Weibull breakdown field measurement

Polymer	Weibull characteristic breakdown field (MV m^{-1})	Slope	Quality of fit (R^2)	Number of samples
PDTC-ODA	704	9.517	0.965	30
PDTC-MDA	714	10.30	0.923	30
PDTC-HDA	666	20.95	0.955	30
PDTC-HK511	602	6.03	0.971	30
Thiophosgene-MDA	677	19.24	0.927	30

Published on 30 April 2015. Downloaded by University of Connecticut on 09/07/2015 16:10:22.

for the breakdown measurement, with a picture of the film shown as an example. Breakdown fields achieved through *D–E* hysteresis loop is comparable with the value from linear DC voltage ramp in Table 4, with the results for PTDC-HDA as an example in Fig. 3 (the *D–E* loops for other polymers are reported in the ESI†). A high released energy density of 9.3 J cm^3 was achieved for PDTC-HDA with a breakdown strength of ~685 MV m^{-1}. Hysteresis observed in the *D–E* loops is believed to be originated from conduction loss at high voltage, which can be attributed to residue solvent and other impurities. The films were prepared through industrial scale processing, which produces large scale free standing films. The casting speed, drying condition and thermal annealing all lead to different surface structure and defect levels. Large scale processing brought a higher level of surface roughness and more defects and impurities, which reduced efficiency and breakdown voltage. However, large scale free standing films are required for capacitor assembling. Further optimization of processing conditions will be conducted to improve the overall performance. Refined high field conduction study will be performed to champion the thin film processing optimization.

Conclusions

A systematic study on polythioureas was conducted as a prospective dielectric layer by implementation of a high throughput hierarchical modelling with combinatorial exploration and successive screening, followed by an evolutionary structure search based on density functional theory (DFT). From a downselection, a series of polythioureas were synthesized and investigated in terms of dielectric constant and loss, band gap, charge–discharge behaviour and DC breakdown strength. A dielectric constant of ~4.5 and a corresponding energy density of ~10 J cm^{-3} were achieved in accordance with Weibull characteristic breakdown voltage of ~700 MV m^{-1}. With the incorporation of various chain segments, including aromatic, aliphatic and polyether, we were able to tune dielectric properties by means of introducing additional permanent dipoles, altering conjugation length, controlling morphology, *etc.* Crystalline structures in solution casted films were observed by WAXD (Wide Angle X-ray Diffraction), which were in great agreement with DFT predicted diffraction patterns. The effects of crystalline structure, microstructure and processing conditions on high voltage conduction loss and breakdown strength were also discussed.

Experimental

1. Materials and synthesis

Para-phenylene diisothiocyanate (PDTC), thiophosgene, 1,4-diazabicyclo [2.2.2]octane (DABCO), 4,4′-oxydianiline (ODA), 4,4′-diphenylmethanediamine (MDA), 1,4-diaminobenzene (PhDA), 1,6-diaminohexane (HDA) and anhydrous *N*-methyl-2-pyrrolidone (NMP), dimethyl sulfoxide (DMSO), dimethylacetamide (DMAc) were all purchased from Sigma-Aldrich Chemical Company. DABCO was recrystallized from petroleum ether before use, whereas all other chemicals were used as received.

Polythioureas were prepared through two synthetic methods: (1) the reaction of diamine with diisothiocyanate or (2) the reaction of diamine with thiophosgene. For method (1), *p*-phenylene diisothiocyanate was added in the NMP solution of diamine while stirring under inert atmosphere. After 6 h at room temperature, the reaction mixture was poured into methanol with fibre-like precipitation, followed by washing with methanol and dried at 50 °C *in vacuo* overnight. For method (2), the reaction was carried out in a completely dried four neck flask equipped with dropping funnel, distillation and safety trap. Thiophosgene was carefully and slowly added to the mixture of DABCO and diamine in NMP at 0 °C. The reaction was carried out at room temperature for 24 h after reactants were well mixed. Deionized water and methanol was used for precipitation and washing. Polymer was obtained after purification and drying 50 °C *in vacuo* (details for each polymer in ESI†).

2. Measurements and instruments

Fourier Transform Infrared (FTIR) spectra were recorded with a Nicolet Magna 560 FTIR spectrometer (resolution 0.35 cm^{-1}). Solution ^{1}H NMR was performed on a Bruker DMX500 high resolution digital NMR spectrometer. Thermogravimetric analysis (TGA) was performed with TA instruments TGA Q500 (heating rate 10 °C min^{-1} under nitrogen), and differential scanning calorimetry (DSC) analysis was performed by TA instrument DSC Q-100 with the glass transition and melting point determined from the second heating cycle at 10 °C min^{-1}. The diffraction data was recorded on an Oxford Diffraction Xcalibur PX Ultra with a Cu-Kα (λ = 0.15418 nm).

Polythiourea films with thickness ~10 μm were prepared by casting solution on borosilicate glass plates using Erichsen CoatMaster Film Applicator with fixed blade gaps for different polymers. Free standing films peeled off of the glass substrate were dried *in vacuo* to remove residue solvent and anneal (detailed description for each polythiourea in ESI†).

Dielectric spectroscopies were obtained using an IMASS Time Domain Dielectric Spectrometer. Measurements were made in an air circulating oven at constant temperature by taking frequency scans, with 10 volts AC applied. Polarization measurements were conducted with a modified Sawyer-Tower circuit, employing a Trek Model 10/40 10 kV high voltage amplifier and an OPA541 operational amplifier based current to voltage converter. The samples were sputtered with Au/Pd 80/20 wt% electrodes of 0.07 cm^2. The UV-vis spectrum for band gap determination was obtained using Varian Cary UV-VIS 5000. The UV-vis spectra were recorded from 200–800 nm and the onset wavelength of absorption, λ_{onset}, was used to determine the band gap (E_g) from Planck's equation: $E_g = hc/\lambda_{onset}$. The refractive index was evaluated using variable angle spectroscopic ellipsometry (VASE, J.A.Woollam Co., M-2000). General scans were performed over the wavelength range from 350 to 1497 nm, values at 546 nm listed in Table 3. The ellipsometric angles were modelled using a recursive model consisting of the silicon substrate and a Cauchy layer to describe the refractive index of films. Breakdown strength measurements were

 This journal is © The Royal Society of Chemistry 2015

Published on 30 April 2015. Downloaded by University of Connecticut on 09/07/2015 16:10:22.

performed using a linear voltage ramp generated by a resistor capacitor (RC) circuit. When the first breakdown event occurs, the power supply is shut off through an interlock input by a silicon controlled rectifier (SCR) circuit, which uses the breakdown-induced ground-rise voltage capacitively coupled to the gate of an SCR. The breakdown voltage of the sample is read from a peak-holding voltmeter. The sample thickness was determined using a thickness gauge (Model LE1000-2, MeasureItAll) as the average of several measurements near the breakdown site.

3. Calculation methodology

The quantum mechanical computations were performed using density functional theory (DFT) as implemented in the Vienna *ab initio* software package. The generalized gradient approximation (GGA) functional parameterized by Perdew, Burke and Ernzerhof (PBE) to treat the electronic exchange–correlation interaction, the projector augmented wave (PAW) potentials, and plane-wave basis functions up to a kinetic energy cutoff of 500 eV were employed. The supercells were relaxed using a conjugate gradient algorithm until the forces on all atoms were <0.02 eV Å^{-1}. As the PBE functional is known to underestimate band gaps of insulators, the Heyd–Scuseria–Ernzerhof HSE06 functional was used to obtain corrected band gap values for all systems considered.

In order to identify 3-dimensional structure of polymers and provide a more accurate prediction on dielectric properties, van der Waals interactions were taken into account using the vdW-TS functional. Phonon dispersion curves were calculated using the supercell approach with the finite displacement method as implemented in the PHONOPY code, while FullProf suite was used to simulate the X-ray diffraction patterns. A specifically designed constrained evolutionary algorithm, embodied in the USPEX code was used to predict polymeric crystal structures starting from the single polymeric chains discussed above (using first principles quantum mechanical computations for the total ground state energy of the crystals). This newly developed method uses a specification of well-defined molecular repeat units rather than individual atoms as the starting point. The diversity of the population of structures is enhanced by using space group symmetry combined with random cell parameters, and random positions and orientations of molecular units. During the evolutionary optimization, structures with different sequence and packing of these repeat units are generated and relaxed. We performed multiple runs of evolutionary search with 2 and 4 repeat units. The total energies were obtained with the PBE exchange–correlation functionals using the dispersion correction prescribed by the vdW-TS approach. In all cases considered here, the energetic orderings are invariant with respect to the choice of different exchange–correlation functions.

Acknowledgements

This work was supported by a Multi-University Research Initiative (MURI) grant from the Office of Naval Research, under award number N00014-10-0944. The authors thank JoAnne Ronzello for performing the TDDS measurements.

Notes and references

1 F. Beach and I. McNab, *IEEE Trans. Magn.*, 2005, **3**(12), 1.
2 I. Husain, *Electric and Hybrid Vehicles: Design Fundamentals*, CRC Press, Boca Raton, FL, 2010.
3 R. Teodorescu, M. Liserre and P. Rodríguez, *Grid Converters for Photovoltaic and Wind Power Systems*, Wiley, Chichester, 2011.
4 H. Bluhm and D. Rusch, *Pulsed Power Systems: Principles and Applications*, Springer, Berlin, 2006.
5 M. Winter and R. Brodd, *J. Chem. Rev.*, 2004, **104**, 4245.
6 W. J. Sarjeant, J. Zirnheld and F. W. MacDougall, *IEEE Trans. Plasma Sci.*, 1998, **26**, 1368.
7 Q. Tan, P. Irwin and Y. Cao, *IEEJ Trans. Fundam. Mater.*, 2006, **126**, 1153.
8 B. Chu, X. Zhou, K. Ren, B. Neese, M. Lin, Q. Wang, F. Bauer and Q. M. Zhang, *Science*, 2006, **313**, 334.
9 Q. Chen, Y. Wang, X. Zhou, Q. M. Zhang and S. Zhang, *Appl. Phys. Lett.*, 2008, **92**, 142909.
10 N. Balke, M. Gajek, A. K. Tagantsev, L. W. Martin, Y.-H. Chu, R. Ramesh and S. V. Kalinin, *Adv. Funct. Mater.*, 2010, **20**, 3466.
11 W. J. Sarjeant, F. W. MacDougall and D. W. Larson, *IEEE Electr. Insul. Mag.*, 1997, **13**, 20.
12 M. Rabuffi and G. Picci, *IEEE Trans. Plasma Sci.*, 2002, **30**, 1939.
13 G. Picci and M. Rabuffi, *IEEE Trans. Plasma Sci.*, 2000, **28**, 1603.
14 E. J. Barshaw, J. White, M. J. Chait, J. B. Cornette, J. Bustamante, F. Folli, D. Biltchick, G. Borelli, G. Picci and M. Rabuffi, *IEEE Trans. Magn.*, 2007, **43**(1), 223.
15 J. Ho, R. Ramprasad and S. Boggs, *IEEE Trans. Dielectr. Electr. Insul.*, 2007, **14**, 1295.
16 J. H. W. Starkweather, P. Avakian, R. R. Matheson, J. J. Fontanella and M. C. Wintersgill, *Macromolecules*, 1992, **25**, 6871.
17 V. Tomer and C. A. Randall, *J. Appl. Phys.*, 2008, **104**, 074106.
18 P. Kim, N. M. Doss, J. P. Tillotson, P. J. Hotchkiss, M. J. Pan, S. R. Marder, J. Li, J. P. Calame and J. W. Perry, *ACS Nano*, 2009, **3**, 2581.
19 J. Li, J. Claude, L. E. Norena-Franco, S. I. Seok and Q. Wang, *Chem. Mater.*, 2008, **20**, 6304.
20 N. Guo, S. A. DiBenedetto, P. Tewari, M. T. Lanagan, M. A. Ratner and T. Marks, *J. Chem. Mater.*, 2010, **22**, 1567.
21 J. P. Calame, *J. Appl. Phys.*, 2006, **99**, 084101.
22 A. L. An and S. A. Boggs, *Proceedings of the 2006 IEEE International Symposium on Electrical Insulation*, Toronto, June 2006.
23 B. Chu, X. Zhou, K. Ren, B. Neese, M. Lin, Q. Wang, F. Bauer and Q. M. Zhang, *Science*, 2006, **313**, 334.
24 F. Guan, J. Pan, J. Wang, Q. Wan and L. Zhu, *Macromolecules*, 2010, **43**, 384.
25 W. Li, L. Jiang, X. Zhang, Y. Shenb and C. W. Nan, *J. Mater. Chem. A*, 2014, **2**, 15803.

Published on 30 April 2015. Downloaded by University of Connecticut on 09/07/2015 16:10:22.

26 A. F. Baldwin, R. Ma, C. C. Wang, R. Ramprasad and G. A. Sotzing, *J. Appl. Polym. Sci.*, 2013, **130**, 1276.
27 R. Ma, A. F. Baldwin, C. C. Wang, R. Ramprasad and G. A. Sotzing, *ACS Appl. Mater. Interfaces*, 2014, **6**(13), 10445.
28 I. Treufeld, D. H. Wang, B. A. Kurish, L. Tan and L. Zhu, *J. Mater. Chem. A*, 2014, **2**, 5244.
29 V. Sharma, C. Wang, R. G. Lorenzini, R. Ma, Q. Zhu, D. W. Sinkovits, G. Pilania, A. R. Oganov, S. Kumar, G. A. Sotzing, S. A. Boggs and R. Ramprasad, *Nat. Commun.*, 2014, **5**, 4845.
30 S. Wu, W. Li, M. Lin, Q. Burlingame and Q. M. Zhang, *Adv. Mater.*, 2013, **25**, 1734.
31 L. Zhu, *J. Phys. Chem. Lett.*, 2014, **5**, 3677.
32 A. F. Baldwin, R. Ma, A. Mannodi-Kanakkithodi, T. D. Huan, C. Wang, M. Tefferi, J. E. Marszalek, M. Cakmak, Y. Cao, R. Ramprasad and G. A. Sotzing, *Adv Mater.*, 2015, **27**(2), 346.
33 C. C. Wang, G. Pilania, S. A. Boggs, S. Kumar, C. Breneman and R. Ramprasad, *Polymer*, 2014, **55**, 979.
34 A. R. Oganov, *Modern Methods of Crystal Structure Prediction*, Wiley-VCH, 2011.
35 A. R. Oganov and C. W. Glass, *J. Chem. Phys.*, 2006, **124**, 244704.
36 Q. Zhu, V. Sharma, A. R. Oganov and R. Ramprasad, *J. Chem. Phys.*, 2014, **141**, 154102.
37 J. Liub and M. Ueda, *J. Mater. Chem.*, 2009, **19**, 8907.
38 Y. Sun, C. Bealing, S. A. Boggs and R. Ramprasad, *IEEE Electr. Insul. Mag.*, 2013, **29**, 8.
39 L. A. Dissado and J. C. Fothergill, *Electrical Degradation and Breakdown in Polymers*, Peter Peregrinus Ltd., London, 1992, part 3.
40 Y. Sun, S. A. Boggs and R. Ramprasad, *IEEE Trans. Dielectr. Electr. Insul.*, 2015, **22**(1), 495.

This journal is © The Royal Society of Chemistry 2015